ASTFE
American Society
of Thermal and Fluids Engineers

10th Thermal and Fluids Engineering Conference (TFEC)
March, 9-12, 2025
Partially Online Virtual and at George Washington University, DC, USA

TFEC-2025-56049

COMPRESSIBILITY EFFECT ON POD MODES OVER ZERO-PRESSURE GRADIENT FLAT PLATE TURBULENT BOUNDARY LAYERS

Subhajit Roy* **& Guillermo Araya**

Computational Turbulence and Visualization Lab., Department of Mechanical, Aerospace, & Industrial Engineering, University of Texas at San Antonio, TX 78249, USA.

ABSTRACT

This work investigates the compressibility effects on Proper Orthogonal Decomposition (POD) modes in spatially developing zero-pressure gradient (ZPG) flat plate turbulent boundary layers using Direct Numerical Simulation (DNS) data [1, 2]. Focusing on three different flow regimes: incompressible, subsonic (Mach 0.8), and supersonic (Mach 1.6), while maintaining a constant Reynolds number, the analysis aims to isolate the effect of increasing Mach numbers on turbulent structures and flow statistics. POD methods are employed to decompose the turbulent flow field into its most energetic modes, providing insight into the changes in coherent structures as the flow transitions from subsonic to supersonic regimes. The inclusion of multiple Mach numbers allows a detailed comparison of flow physics across different compressibility levels. At low Mach numbers, the flow exhibits classical incompressible behavior, while higher Mach numbers introduce compressibility effects such as density variations and rapid energy transfer, which can significantly alter turbulence characteristics. By analyzing the POD modes, the study explores how energy distribution among modes evolves with compressibility. By comparing the modal dynamics across these Mach numbers, we identify key compressibility-driven changes in the coherent structures and energy distribution, contributing to a deeper understanding of boundary layer stability and transition phenomena in compressible flows. These findings have significant implications for high-speed flow applications, especially in aerospace engineering, where boundary layer behavior is critical for performance optimization.

KEY WORDS: Compressibility effect, Proper Orthogonal Decomposition (POD), Turbulent Coherent Structure, Turbulent Boundary Layers, DNS.

NOMENCLATURE

R_{uu}	time autocorrelation		L_t	integral time scale	(s)
τ	time lag	(s)	ω	frequency	(Hz)
a_n	temporal coefficient		ϕ_n	spatial and temporal modes	
u	velocity vector	(m/s)	C	covariance matrix	
POD	Proper Orthogonal Decomposition		ZPG	zero pressure gradient	
DNS	Direct Numerical Simulation				

*Corresponding Subhajit Roy : subhajit.roy@utsa.edu

1. INTRODUCTION

Turbulence is an inherently chaotic and multi-scale phenomenon that governs fluid motion in a wide range of engineering and natural systems. Among these, the turbulent boundary layer over a flat plate subjected to zero-pressure gradient (ZPG) is one of the most fundamental configurations in fluid dynamics. Despite its geometrical simplicity, the ZPG turbulent boundary layer exhibits complex behavior with flow structures ranging from small-scale eddies to large-scale coherent motions that span significant portions of the boundary layer. These turbulent structures are crucial to understanding heat and momentum transfer in wall-bounded flows, and their characterization remains an area of active research [7].

The zero-pressure gradient turbulent boundary layer over a flat plate is characterized by a range of coherent structures that evolve from the near-wall region to the outer layer of the boundary. In the near-wall region, small-scale structures, such as low-speed streaks and quasi-streamwise vortices, dominate. These structures are responsible for the transport of momentum and play a significant role in wall shear stress. Farther from the wall, larger-scale turbulent motions, such as hairpin vortices and other coherent eddies, contribute to the overall turbulence dynamics. Understanding how these turbulent structures form, evolve and interact remains a critical challenge in boundary layer research [10].

Proper Orthogonal Decomposition (POD) is a well-established technique for analyzing turbulent flows. POD, first introduced by Lumley [8], has been widely used to identify coherent structures in turbulent flows by decomposing the velocity field into a set of orthogonal modes, ranked by their energy content. This technique has been particularly useful in incompressible turbulence research, where it has revealed large-scale structures that dominate the flow field. However, for compressible flows, additional challenges arise due to the presence of acoustic and shock waves, making frequency-domain analyses such as Spectral Proper Orthogonal Decomposition (SPOD) more appropriate. SPOD, developed by Towne et al. [12], is an extension of POD that allows for the identification of coherent structures across different frequency scales over time, making it particularly useful for flows, where frequency-dependent phenomena play a key role. SPOD has been applied in a variety of turbulent flows, from jets and wakes to wall-bounded flows, and has provided critical insights into the dynamics of large-scale coherent motions in boundary layers.

In this study, we employ DNS data from ZPG flat plate boundary layers to perform a detailed analysis using POD (Spectral POD will be applied in a future study and published elsewhere). The DNS approach resolves all relevant turbulent scales without the need for empirical turbulence models, making it ideal for examining the full spectrum of turbulent structures. The flow field is decomposed into orthogonal modes to identify the most energetic structures and to examine their spatial and temporal coherence. The study is conducted at three distinct streamwise locations, including the recycling plane, a critical region where boundary conditions are periodically reset to maintain the integrity of the downstream flow. The results of this study provide new insights into the behavior of turbulent structures in the boundary layer, with implications for improving turbulence models and advancing our understanding of wall-bounded flows.

The POD analyses in this study are complemented by an examination of time autocorrelation functions at different wall-normal locations (y^+). The time autocorrelation function is a fundamental tool for assessing the temporal coherence of turbulent structures. By integrating the time autocorrelation, we can obtain the integral time scale, which provides a measure of how long turbulent eddies persist before being broken down by smaller structures. Previous studies have shown that the near-wall region of a boundary layer is dominated by short-lived structures, while larger, more persistent structures prevail in the outer layer. Understanding the temporal and spectral properties of turbulent structures is critical for improving turbulence models, particularly in the context of Large Eddy Simulation (LES) and Reynolds-Averaged Navier-Stokes (RANS) approaches. These models rely on accurate representations of the turbulent energy cascade and the interactions between different scales of motion. The insights gained from POD and SPOD analyses can inform the development of more accurate subgrid-scale models in LES and improved closure models in RANS.

While many studies have investigated the dynamics of ZPG turbulent boundary layers, the combined use of DNS and POD in the present work offers a more comprehensive view of the flow field. By examining

Table 1 DNS Cases.

Case	M_∞	T_w/T_∞	$Re_{\delta 2}$	δ^+	$L_x \times L_y \times L_z$	Δx^+,Δy^+_{min}/Δy^+_{max}, Δz^+
Incompressible	0	Isothermal	302-582	144-261	$45\delta_{inl} \times 3.5\delta_{inl} \times 4.3\delta_{inl}$	14.7, 0.2/13, 8
Subsonic	0.8	1.115	309-571	146-253	$43\delta_{inl} \times 3\delta_{inl} \times 3\delta_{inl}$	14, 0.18/13.4, 7.8
Supersonic	1.6	1.4557	350-648	148-259	$43\delta_{inl} \times 3\delta_{inl} \times 3\delta_{inl}$	14, 0.2/13, 8

the spatial and temporal coherence of turbulent structures at different streamwise locations and wall-normal distances, this study provides a detailed characterization of the energy distribution in the boundary layer. The results of this work have significant implications for both fundamental turbulence research and practical applications, such as aerodynamic design, where accurate predictions of turbulent boundary layer behavior are crucial. The structure of this manuscript is as follows: The next section (section 2) outlines the methodology used to obtain the DNS data and perform the POD analyses. We then present the results (section 3) of the time autocorrelation analysis, followed by a detailed examination of the POD modes. The manuscript concludes with a discussion of the implications of the findings for turbulence modeling and future research directions.

2. METHODOLOGY

In this section, DNS computational and simulation details, along with a brief background of time autocorrelation, and POD methods, are discussed. These tools are used to analyze the DNS data in the results section (section 3).

2.1 DNS computational details

Unsteady three-dimensional simulations of SDTBL via DNS demand high mesh resolution to resolve even the smallest turbulence scales. Furthermore, the dimensions of the large-scale turbulent motions dictate how large the computational domain should be. Additionally, it requires the prescription of physically sound turbulent inflow conditions to circumvent the space and time consuming laminar-transition computation. We are employing a type of rescaling-recycling technique ([9]) as proposed by [1], and adapted to compressible flow in [2]. The idea is to extract the flow solution (mean and fluctuating flow components) from a downstream plane (so-called "recycle") and to apply scaling laws to absorb the streamwise non-homogeneous condition, to finally re-inject it at the inlet plane. In Figure 1, it can be seen the streamwise locations of the inlet and downstream recycle plane. The reader can access more detailed information at [1, 2]. Direct simulations have been carried out via a highly accurate, very efficient, and highly scalable flow solver. PHASTA is an open-source, parallel, hierarchic (2^{nd} to 5^{th} order accurate), adaptive, stabilized (finite-element) transient analysis tool for the solution of compressible [13] or incompressible flows (Jansen [4]). PHASTA has been extensively validated in a suite of DNS under different external conditions [1**?** , 2]. Turning to boundary conditions, at the wall the classical no-slip condition is imposed for all velocity components. An adiabatic wall condition (T_w/T_r = 1) is prescribed for the thermal field with the ratio T_w/T_∞ = 1.045 and 1.115, respectively, where, T_w is the wall temperature, T_∞ is the freestream temperature and T_r is the adiabatic temperature. The periodicity of the flow field is prescribed in lateral surfaces. Furthermore, freestream values are prescribed on the top surface. Table 1 depicts the characteristics of the evaluated three DNS databases of flat plates in the present study: one incompressible case and two compressible cases (M_∞ = 0.8 and 1.6). Numerical details are reproduced here for readers' convenience. The time steps (Δt^+) in wall units were approximately fixed from 0.15 to 0.4. In all cases, the number of mesh points in the streamwise, wall-normal, and spanwise direction is 440 $\times$ 60 $\times$ 80 (roughly a 2.1-million point mesh). The cases were run in 96 cores in HPE SGI 8600-Gaffney (NAVY, DoD).

2.2 Time autocorrelation

Time autocorrelation is a key statistical tool used to analyze the temporal coherence of turbulent flow structures. It describes how the velocity (or another flow variable) at a given point in space is correlated with itself

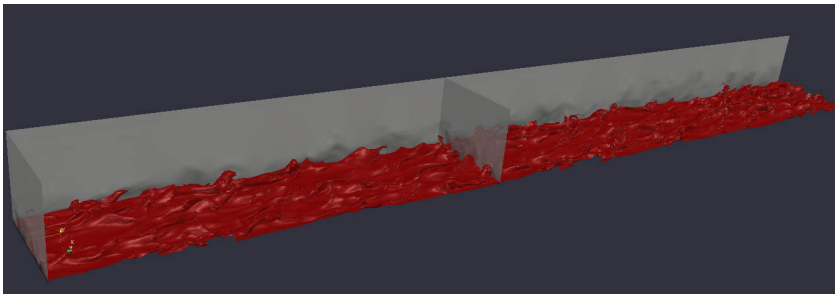

Fig. 1 Boundary layer schematic for the Mach 0.8 case. Iso-surfaces of instantaneous static temperature (in red), contours of instantaneous temperature in extracted planes (flow from left to right).

over a time interval. The autocorrelation function, $R(\tau)$, is defined as the correlation between a signal at a certain time, t, and at a later time, t + τ, where τ is the time lag. In the context of turbulent flows, time autocorrelation functions provide insight into the persistence and lifespan of turbulent eddies at different spatial locations, particularly in boundary layers. For a fluctuating velocity component, $u'(t)$, the time autocorrelation function is expressed as:

$$R_{uu}(\tau) = \frac{\langle u'(t)u'(t+\tau)\rangle}{\langle u'(t)^2\rangle}, \tag{1}$$

where $\langle . \rangle$ denotes an ensemble average or time average for stationary turbulence. The autocorrelation function takes a maximum value of 1 at $\tau = 0$ (where the velocity is perfectly correlated with itself) and decreases as τ increases, indicating a loss of temporal coherence.

Numerous experimental and computational studies have explored the temporal characteristics of turbulent boundary layers through time autocorrelation analysis. Early work by Kline et al. [6] demonstrated the short-lived nature of near-wall structures in low Reynolds number boundary layers. More recent studies by Hutchins and Marusic [3] provided detailed measurements of autocorrelation functions at different wall-normal positions in high Reynolds number flows, showing the persistence of large-scale motions (LSMs) and very-large-scale motions (VLSMs) in the outer layer. Additionally, DNS studies by Jiménez and Moser [5] have examined the role of large-scale structures in temporal coherence and have provided a quantitative basis for understanding the scaling of time scales in turbulent boundary layers. Overall, time autocorrelation functions offer a detailed view of the temporal dynamics of turbulence, from the rapid, short-lived fluctuations near the wall to the more coherent, longer-lasting structures in the outer region. By analyzing these functions at different streamwise and wall-normal locations, researchers can gain a deeper understanding of the complex temporal evolution of turbulent structures in boundary layers.

One of the key parameters derived from the time autocorrelation function is the integral time scale, L_t, which provides a measure of how long the turbulent structures persist. The integral time scale is obtained by integrating the autocorrelation function:

$$L_t = \int_0^\infty R_{uu}(\tau)\, d\tau. \tag{2}$$

The integral time scale is often used as an estimate of the eddy turnover time, or *the time it takes for a turbulent eddy to lose its coherence and break down into smaller eddies*. In turbulent boundary layers, the integral time scale varies with wall-normal distance. Near the wall, the time scales are short due to the rapid decorrelation of near-wall streaks and vortices. In the outer regions, where large-scale motions dominate, the time scales are significantly longer, reflecting the more persistent nature of the turbulent structures.

2.3 Proper orthogonal decomposition (POD)

The application of POD to turbulent flows was pioneered by Lumley (1967), who introduced the idea of decomposing turbulent flow fields into orthogonal modes. This approach has since been applied extensively in experimental and computational fluid dynamics to analyze coherent structures in boundary layers, jets, and wake flows. Sirovich (1987) introduced the "snapshot" POD method, which has become a standard tool for analyzing high-dimensional flow data from DNS and LES. This method has been used to study coherent structures in a wide range of turbulent flows, including boundary layers, channel flows, and jets. Studies by Berkooz et al. (1993) and Holmes et al. (1996) provided further theoretical development and applications of POD in turbulence research.

The goal of POD is to find a set of basis functions that best describe the flow, capturing the most energetic structures in the flow field. The velocity field $u(x,t)$, where x represents the spatial coordinates and t is time, can be decomposed as follows:

$$u(x,t) = \sum_{n=1}^{N} a_n(t)\phi_n(x), \tag{3}$$

where $\phi_n(x)$ orthogonal spatial modes (POD modes), $a_n(t)$ are the temporal coefficients of each mode, and N is the total number of modes. In practical applications, the "snapshot" POD method proposed by Sirovich (1987) is often used. This method is computationally efficient, particularly for high-dimensional data from simulations such as DNS or LES. The velocity field is sampled over time, generating a series of "snapshots," which are used to construct the correlation matrix. The POD modes are then obtained by solving an eigenvalue problem for the correlation matrix. Given M snapshots of the velocity field $u(x,t_i)$, the covariance matrix is defined as:

$$C = \frac{1}{M}\sum_{i=1}^{N} u(x,t_i)u(x,t_i)^T. \tag{4}$$

Solving the eigenvalue problem for C yields the temporal coefficients and the spatial modes.

3. RESULT AND DISCUSSION

Fig. 2 demonstrates the non-dimensional velocity scaling of turbulent boundary layers for both incompressible and compressible (Mach 0.8 and Mach 1.6) cases at three different streamwise locations, indicated by the indices i = 178, 338, 400. These indices correspond to different streamwise locations along the flat plate. The velocity profile is presented in a non-dimensional form where u^+ represents the velocity scaled by the friction velocity u_τ, and y^+ s the non-dimensional wall-normal coordinate defined as $y^+ = \frac{yu_\tau}{\nu_w}$, where ν_w is kinematic viscosity at the wall. The figure illustrates that compressibility has a limited impact on the velocity profiles for both moderate (Mach 0.8) and high-speed (Mach 1.6) flows, suggesting that the flow remains largely subsonic, with Mach number effects not being dominant. This observation supports the hypothesis that the turbulent boundary layer's scaling laws (logarithmic law of the wall) remain valid even in compressible flows up to supersonic speeds. Note that at higher Mach numbers, there is a slight deviation from the incompressible profile, particularly at larger y^+ due to the compressibility effect.

Fig. 3 illustrates the non-dimensional Reynolds stress components as a function of the non-dimensional wall-normal distance, y^+, for all three cases and locations. The normal Reynolds stresses, which are a key indicator of the turbulent fluctuations, are normalized by the friction velocity and the Reynolds shear stress component is normalized by the friction velocity squared. These normalized Reynolds stress components quantify the intensities of the velocity fluctuations in different directions and provide insights into the turbulence structure within the boundary layer. Across all Reynolds stress components, the profiles show self-similarity in

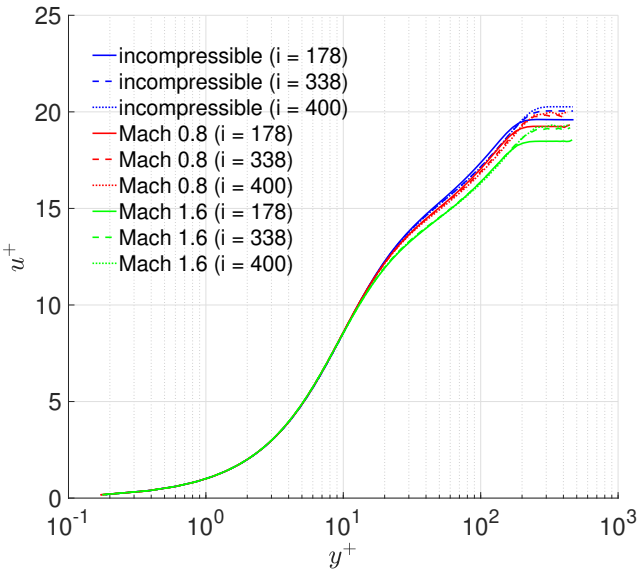

Fig. 2 Velocity profiles along the wall normal direction for incompressible, M = 0.8, and M =1.6 cases at three different streamwise locations.

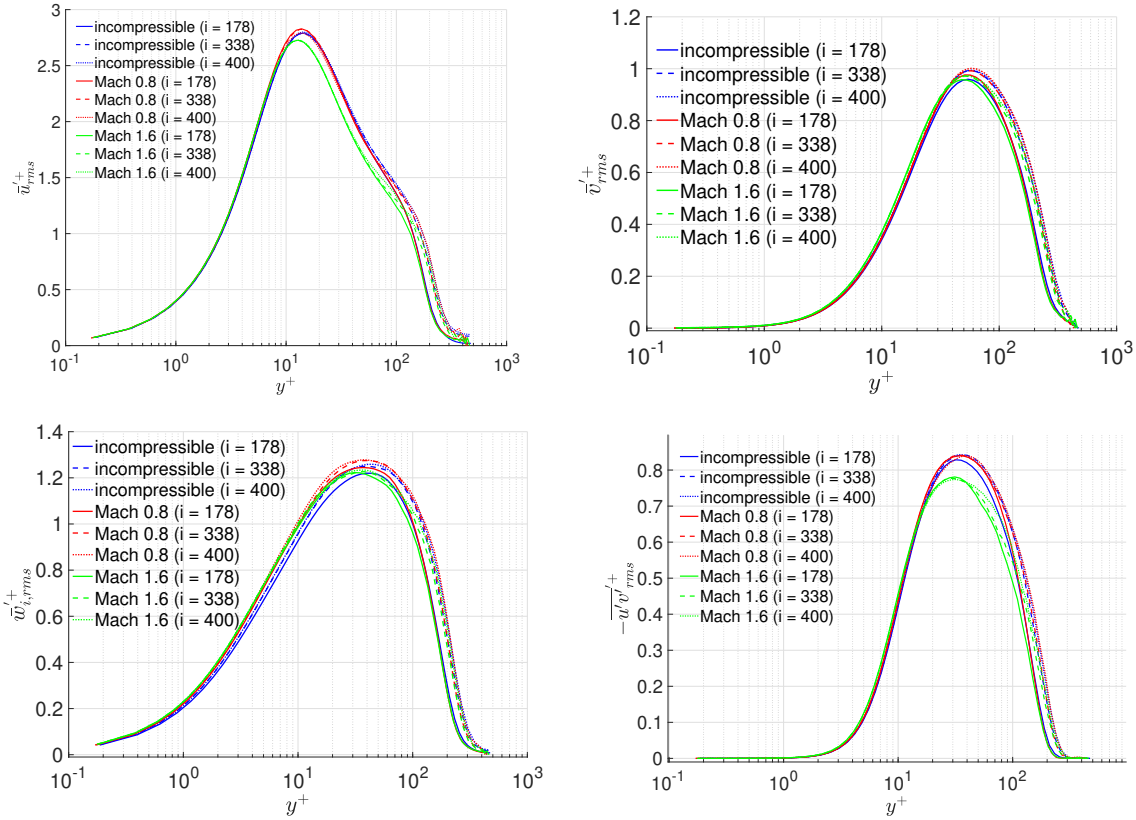

Fig. 3 Reynolds stresses profiles along the wall-normal direction for incompressible, M = 0.8, and M =1.6 cases at three different streamwise locations.

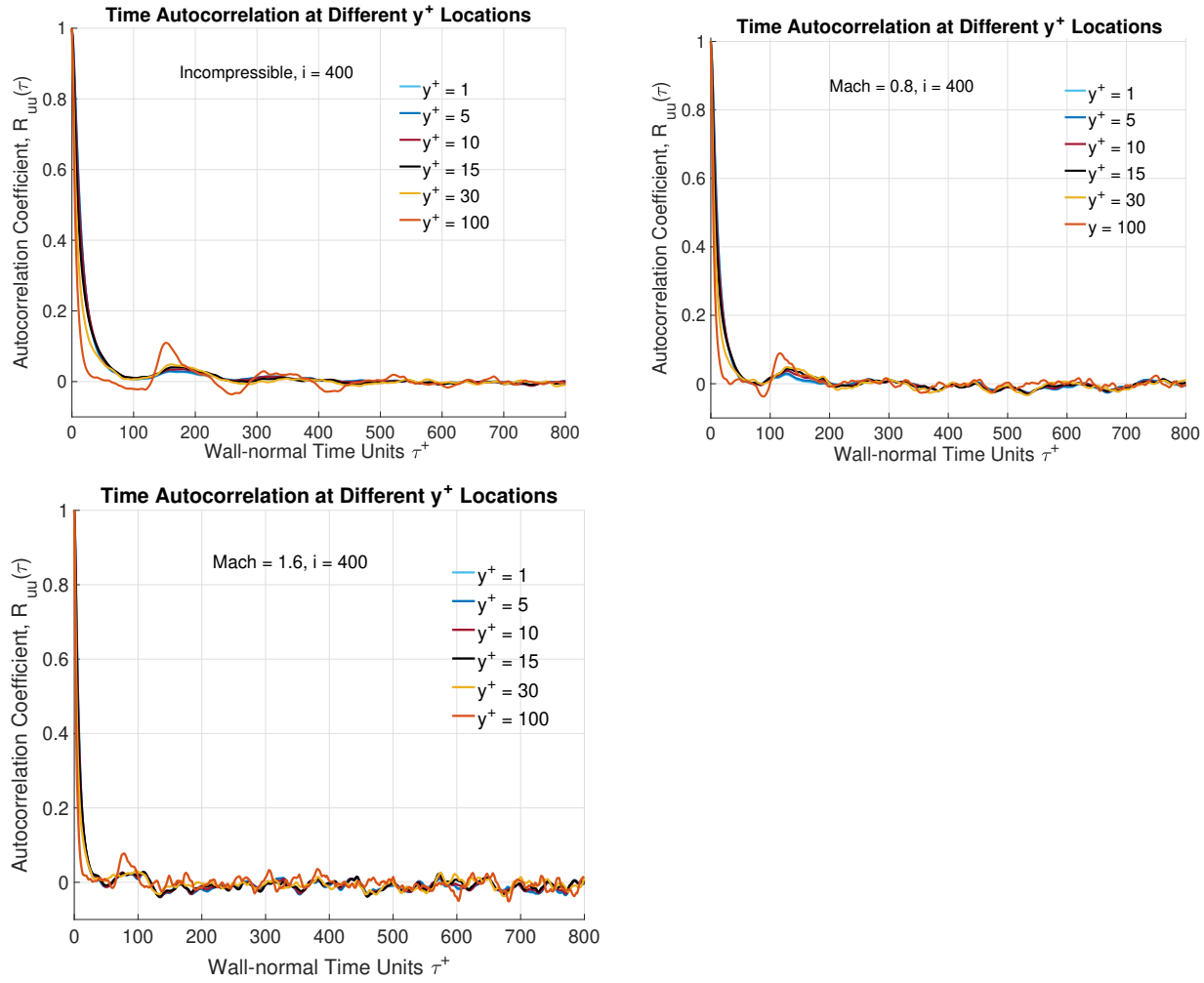

Fig. 4 Velocity time autocorrelation for incompressible, M = 0.8, and M =1.6 cases at $i = 400$ plane.

terms of their shape and distribution, regardless of the Mach number. This suggests that the turbulent structures of the boundary layer remain largely consistent, even at higher Mach numbers, confirming Morkovin's hypothesis [11]: "the essential dynamics of these shear flows will follow the incompressible pattern." The minimal deviations between the compressible (Mach 0.8 and Mach 1.6) and incompressible cases indicate that compressibility has a limited impact on the Reynolds stresses. The slight reductions in the shear stress and streamwise stress at Mach 1.6 could be due to the onset of compressibility effects, but these effects are not dominant in the boundary layer. This result is significant in confirming that the logarithmic law of the wall and the general scaling behavior of turbulence in the boundary layer hold true, even in the presence of compressibility effects.

Fig. 4 presents the time autocorrelation of the streamwise velocity component at different wall-normal locations in the turbulent boundary layer for three cases: incompressible flow, Mach 0.8, and Mach 1.6. The results are presented at a specific streamwise location of $i = 400$. The time autocorrelation function measures the degree of correlation between velocity fluctuations at a given time and velocity fluctuations at later times, as a function of the time separation. It provides insights into the temporal coherence of turbulent structures at different wall-normal positions, revealing how long turbulent structures persist over time at different distances from the wall. For the incompressible case, the autocorrelation decreases sharply as τ^+ increases, indicating that turbulent structures quickly lose coherence over time. At the near-wall region ($y^+ < 5$), the autocorrelation drops to near-zero values within approximately 100 wall-normal time units. The presence of local peaks

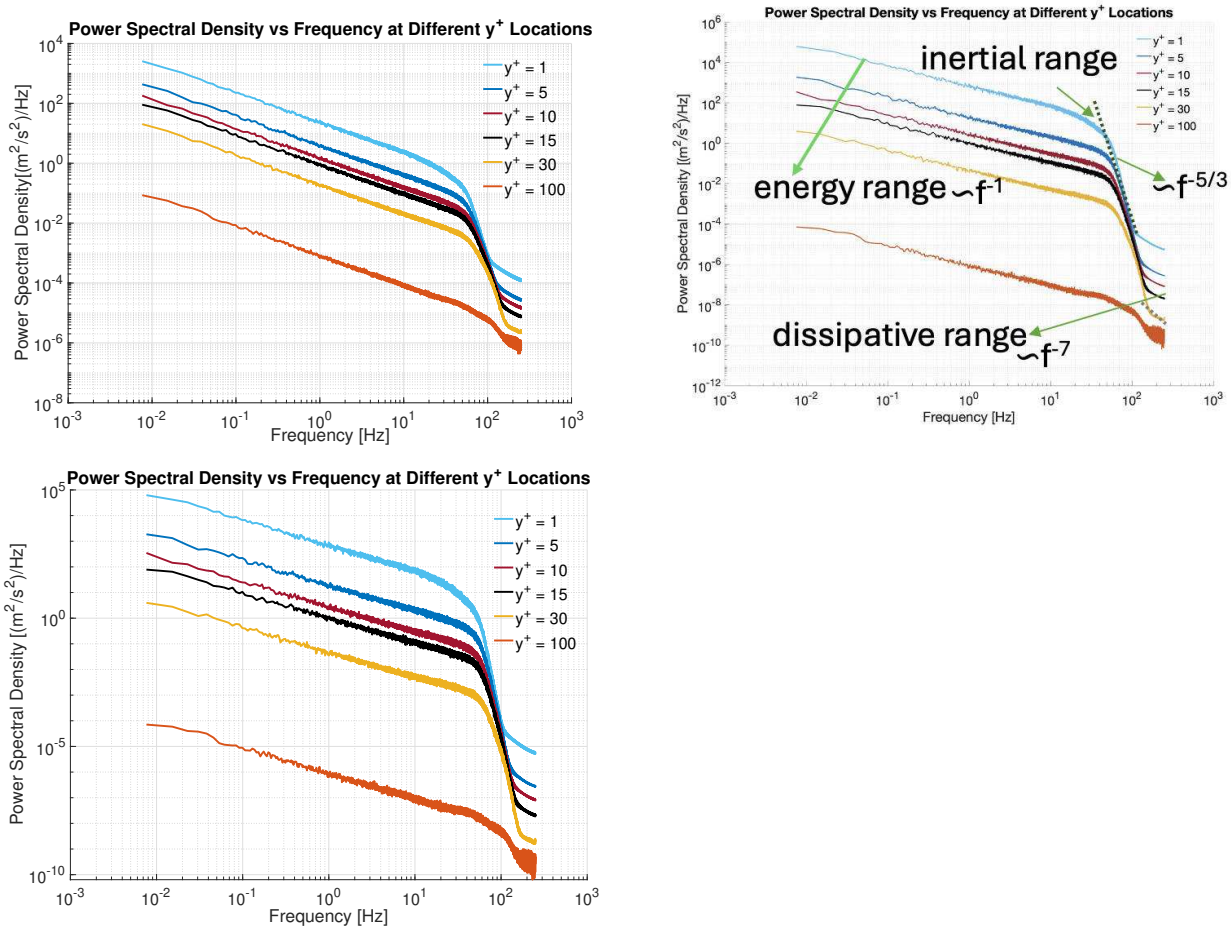

Fig. 5 Power spectral density (PSD) of streamwise velocity fluctuation (u') for incompressible (top-left), M = 0.8 (top-right), and M = 1.6 (bottom) cases at i = 400 plane.

in time-autocorrelation can be attributed to periodic events due to the recycling technique for turbulent inflow generation. Those periodic events quickly decay beyond $\tau^+ = 200$. As we move farther from the wall, the decay is faster, showing that turbulent structures retain their coherence for a shorter time. The curves plateau at small negative values beyond $\tau^+ = 100$, indicating that velocity fluctuations become uncorrelated and random.

For the compressible case at Mach 0.8, the autocorrelation also decays rapidly, similar to the incompressible case. However, the decay is slightly faster, particularly at the higher y^+ locations. The correlation drops to zero in the near-wall region around 50-70 wall-normal time units. The shorter temporal coherence in this case suggests that compressibility effects reduce temporal coherence. In the Mach 1.6 case, the decay of auto-correlation is more pronounced compared to both incompressible and Mach 0.8 cases. High compressibility reduces the temporal coherence of velocity fluctuations even further, especially in the near-wall region. Note that, the time autocorrelation for the temperature field and other streamwise locations follows a similar pattern and is not presented here for brevity. For all cases, near wall locations ($y^+ = 1$) show sharp initial decay, attributed to the high-frequency, small-scale turbulent structures in the viscous sublayer. The decay is slower at the higher y^+ due to the influence of larger, more coherent structures in the outer layer.

Fig. 5 shows the power spectral density of streamwise velocity fluctuations at varying frequencies for different y^+ values. The figure corresponds to all three cases at the i = 400 plane. The figure reveals the distribution

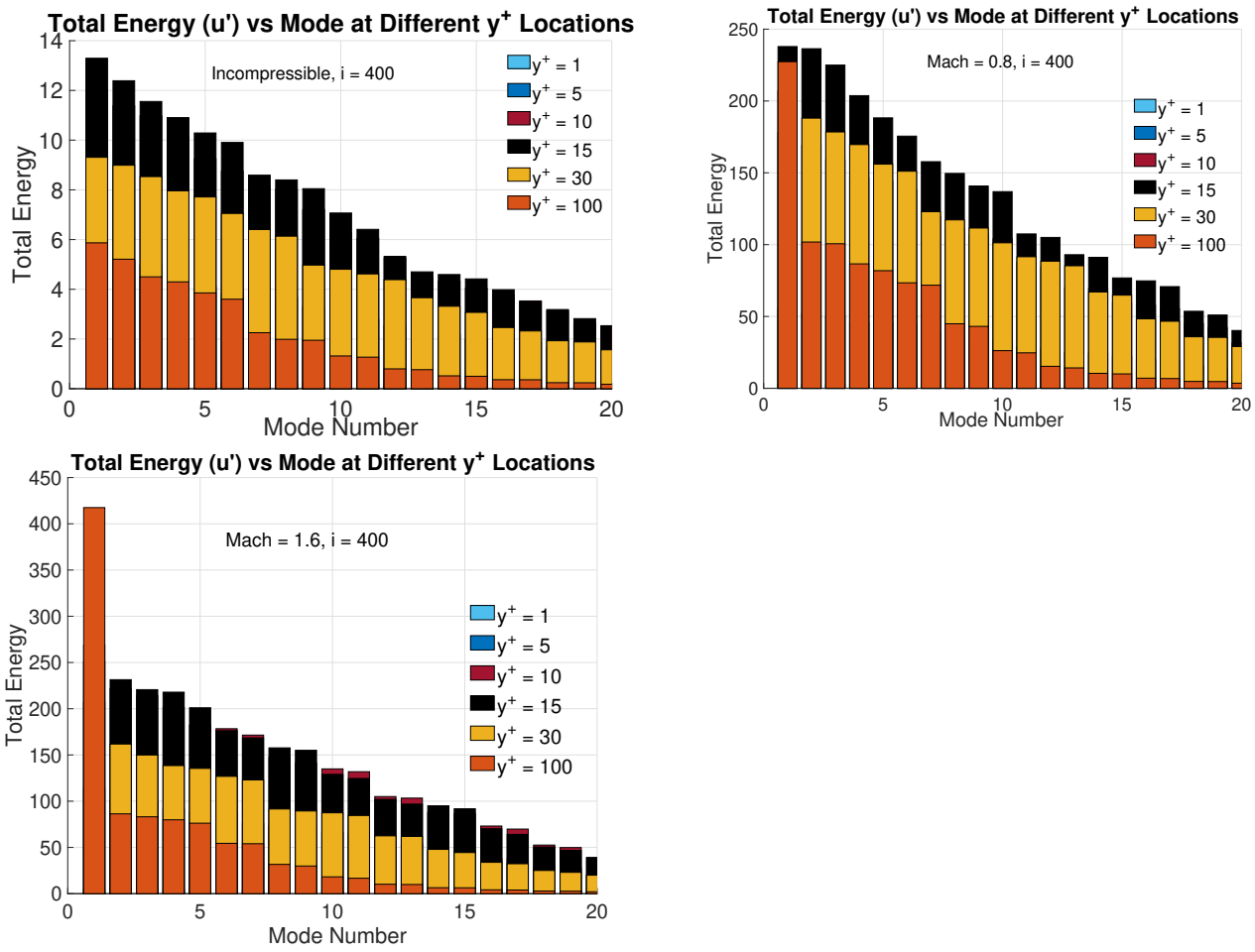

Fig. 6 Total energy distribution vs mode number for incompressible, M = 0.8, and M =1.6 cases at i = 400 plane.

of energy across scales in the turbulent flow, with frequency acting as an evaluator for eddy size (low frequencies correspond to large eddies, and high frequencies to small eddies). The low-frequency range (scales as f^{-1}) represents large-scale energy-containing eddies that dominate turbulence in the regions near the wall. These structures are responsible for most of the turbulent kinetic energy (TKE) and momentum transfer in the boundary layer. In the intermediate frequency range, the power spectral density follows a scaling $f^{-5/3}$, consistent with the Kolmogorov theory of homogeneous turbulence. This indicates that the energy transfer between scales occurs without dissipation. This range is commonly referred to as the inertial subrange, where energy cascades from large eddies to smaller ones without significant viscous effects. The inertial range is limited to $y^+ = 100$, suggesting that energy transfer is less efficient in the outer regions of the boundary layer. At higher frequencies, the PSD shows a steep decay, following a scaling f^{-7}. This region represents the dissipation of turbulent energy into heat as a result of viscous effects. The dissipation of energy at high frequencies is critical for understanding how turbulence loses energy and transitions from turbulent to laminar or less turbulent states. These spectral distributions align with classical turbulence theory, where large structures form near the wall and progressively break down into smaller structures through the energy cascade process. This plot clearly illustrates the scale separation in turbulent flows and how the energy associated with different frequencies changes with the wall-normal distance. The results here also reinforce the known hierarchy of eddies in wall-bounded turbulent flows: large-scale motions near the wall and smaller-scale motions farther from the wall.

Fig. 6 depicts the total energy distributed between POD modes for different values of y^+ for all three cases at the i = 400 location. The total energy is calculated using the streamwise velocity fluctuation, and only the first 20 modes from the POD analysis are shown here for comparison. The mode number corresponds to different scales of turbulent structures in the flow. The lower modes (e.g., modes 1–5) represent the largest and most energetic structures, while the higher modes correspond to smaller and less energetic structures. In all cases, the energy decreases as the mode number increases, meaning that the largest modes contain the majority of the flow energy. For the incompressible case, the total energy is relatively low, with the highest energy seen in the lowest modes. The energy drop-off is more gradual across the modes compared to the compressible cases. The highest energy contains between y^+ = 15-100, suggesting the dominance of large, coherent structures in the buffer and the initial part of the log region of the boundary layer. For the subsonic Mach 0.8 case, the overall energy levels are significantly higher than in the incompressible case, particularly in the region between y^+ = 15 and 100. The energy content in the higher modes is slightly higher than in the incompressible case, suggesting that compressibility effects introduce more energy into the smaller scales.

The supersonic case (Mach 1.6) shows the highest energy levels, especially in the first few modes. The total energy in each mode is significantly higher compared to the other two flow conditions. There is a more pronounced drop-off in energy for higher modes, suggesting that, despite the increased energy at higher Mach numbers, large-scale structures remain the primary contributors to the flow energy. The effects of compressibility are more evident here, as energy is distributed more widely across modes than in incompressible and subsonic cases, possibly due to bulk compression or dilatation, and other high-speed phenomena contributing to turbulent energy. Note that the large energy distribution is also observed at y^+ = 10 for the supersonic case at a high mode number due to the compressibility effect. The energy distribution at other streamwise locations as well as for the thermal field (not shown) follow a similar trend with a significant compressibility effect observed at high Mach numbers.

4. CONCLUSION

This study has provided an in-depth analysis of the compressibility effects on POD modes over ZPG turbulent boundary layers at three distinct Mach numbers: incompressible, 0.8, and 1.6. By maintaining a constant Reynolds number, we isolated the influence of Mach number on the turbulent structures and energy distribution, offering new insights into how compressibility modifies the characteristics of turbulence in boundary layer flows. The results demonstrate that compressibility plays a significant role in redistributing energy across different turbulence scales, with notable effects on both the spatial coherence and frequency-dependent behavior of the flow. One key finding is the substantial alteration in the turbulent energy content and mode distribution as the Mach number increases. This suggests that traditional turbulence models, which assume incompressible behavior or rely on Morkovin's hypothesis, may not be sufficient to capture the complexities of high-speed flows. The presence of significant high-frequency structures at higher Mach numbers also highlights the importance of accurately modeling compressibility effects in turbulence simulations, especially in applications involving supersonic and hypersonic flows. Future work will focus on extending the analysis to a broader range of Reynolds numbers and investigating the impact of different boundary conditions, such as pressure gradients, surface roughness, and wall thermal conditions on the turbulence dynamics. The comprehensive understanding of compressibility effects on turbulent structures, provided by this study, marks a step forward in addressing the challenges of predicting and modeling high-speed turbulent flows.

ACKNOWLEDGMENTS

This material is based upon work supported by the National Science Foundation under grant #2314303. This material is based on research sponsored by the Air Force Research. Laboratory, under agreement number FA9550-23-1-0241. This work was supported in part by a grant from the DoD High-Performance Computing Modernization Program (HPCMP).

REFERENCES

[1] Araya, G., Castillo, L., Meneveau, C., and Jansen, K., (2011) " A dynamic multi-scale approach for turbulent inflow boundary conditions in spatially evolving flows," *Journal of Fluid Mechanics*, 670, pp. 518–605.

[2] Araya, G., Lagares, C., and Jansen, K., (2020) "Reynolds number dependency in supersonic spatially-developing turbulent boundary layers," *AIAA SciTech Forum (AIAA 3247313) Orlando, FL.*, 1.

[3] Hutchins, N. and Marusic, I., (2007) "Large-scale influences in near-wall turbulence," *Philosophical Transactions of the Royal Society A: Mathematical, Physical and Engineering Sciences*, 365(1852), pp. 647–664.

[4] Jansen, K. E., (1999) "A stabilized finite element method for computing turbulence," *Comp. Meth. Appl. Mech. Engng.*, 174, pp. 299–317.

[5] Jiménez, J., Del Alamo, J. C., and Flores, O., (2004) "The large-scale dynamics of near-wall turbulence," *Journal of Fluid Mechanics*, 505, pp. 179–199.

[6] Kline, S. J., Reynolds, W. C., Schraub, F. A., and Runstadler, P. W., (1967) "The structure of turbulent boundary layers," *Journal of Fluid Mechanics*, 30(4), pp. 741–773.

[7] Lele, S. K., (1994) "Compressibility effects on turbulence," *Annual review of fluid mechanics*, 26(1), pp. 211–254.

[8] Lumley, J. L., (1967) "The structure of inhomogeneous turbulent flows," *Atmospheric turbulence and radio wave propagation*, pp. 166–178.

[9] Lund, T., Wu, X., and Squires, K., (1998) "Generation of turbulent inflow data for spatially-developing boundary layer simulations," *Journal of Computational Physics*, 140(2), pp. 233–258.

[10] Martin, M. P., (2007) "Direct numerical simulation of hypersonic turbulent boundary layers. part 1. initialization and comparison with experiments," *Journal of Fluid Mechanics*, 570, pp. 347–364.

[11] Morkovin, M., (1962) "Effects of compressibility on turbulent flows," *Mecanique de la Turbulence*, pp. 367–380.

[12] Towne, A., Schmidt, O. T., and Colonius, T., (2018) "Spectral proper orthogonal decomposition and its relationship to dynamic mode decomposition and resolvent analysis," *Journal of Fluid Mechanics*, 847, pp. 821–867.

[13] Whiting, C. H., Jansen, K. E., and Dey, S., (2003) "Hierarchical basis in stabilized finite element methods for compressible flows," *Comp. Meth. Appl. Mech. Engng.*, 192(47-48), pp. 5167–5185.